**Geomechanics and Engineering**, *Vol. 29, No. 6 (2022) 697-706*
https://doi.org/10.12989/gae.2022.29.6.697


# Research on reinforcement mechanism of soft coal pillar anchor cable

Ang Li*[1], Bingnan Ji[1], Haifeng Zhou[1,5], Feng Wang[3], Yingjie Liu[2], Pengfei Mu[4], Jian Yang[4], Ganggang Xu[4] and Chunhu Zhao[4]

[1]*School of Architecture and Civil Engineering, Xi'an University of Science and Technology, Xi'an, Shaanxi 710054, China*
[2]*Research Institute of Emergency Science, China Coal Research Institute, Beijing 100013, China*
[3]*Shaanxi Coal Chemical Industry Group Chenghe Mines Co., Ltd, Weinan, Shaanxi 715200, China*
[4]*Xi' an Research Institute of China Coal Technology & Engineering Group Corp, Xi' an, Shaanxi 710077, China*
[5]*Shenhua Shendong Coal Group Co., Ltd., Yulin, Shaanxi 719315 China*

*(Received August 23, 2021, Revised April 16, 2022, Accepted April 23, 2022)*

**Abstract.** In order to explore the stable anchoring conditions of coal side under the mining disturbance of soft section coal pillar in Wangcun Coal Mine of Chenghe Mining Area, the distribution model of the anchoring support pressure at the coal pillar side was established, using the strain-softening characteristics of the coal to study the distribution law of anchoring coal side support pressure. The analytical solution for the reinforcement anchorage stress in the coal pillar side was derived with the inelastic state mechanical model. The results show that the deformation angle of the roadway side and roof increases with the roof subsidence due to the mining influence at the adjacent working face, the plastic deformation zone extends to the depth of the coal side, and the increase of anchorage stress can effectively control the roof subsidence and further deterioration of plastic zone. The roadway height and the peak support pressure have a certain influence on the anchorage stress, the required anchorage stress of the coal side rises with the roadway height and the peak support pressure. The required anchorage stress of the coal pillar side decreases as the cohesion between the coal seam and the roof and floor and the anchor length increases. Then, applied the research result to Wangcun coal mine in Chenghe mining area, the design of anchor cable reinforcement support was proposed for the section of coal pillars side that has been anchored and deformed, which achieved great results and effectively controlled the convergence and deformation of the side, providing a safety guarantee for the roadway excavation and mining.

**Keywords:** anchor cable reinforcement; elastic-plasticity; peak support pressure; section coal pillar

## 1. Introduction

Study on the stability of coal pillars are very important to protect the safety of underground workers (Chen *et al.* 2018, Gao 2018). The coal seam in the eastern mine field of Chenghe mining area is generally soft (Li *et al.* 2020a, b, Wei *et al.* 2018). The coal pillars between working faces are often affected by the adjacent mining area resulting in serious deformation of the roadway side and a large plastic deformation range. The deformation of the coal side is close to the anchorage section or exceeds the effective reinforcement range of the anchor, resulting in large area failure of the original support of the roadway, and even instability deformation, as shown in Fig. 1. Previously, the reinforcement was not effective by simply increasing the number of gang anchors (Chen *et al*. 2020), which seriously affected the normal use of the roadway and endangered the safety of underground personnel.

The stability of coal pillars has been studied by many scholars, Wattimena *et al*. (2013) used the logistic regression to calculate draw isoprobability contours, which can quantify the instability probability of coal pillars; Ma *et al.* (2020) used a comprehensive research method including numerical simulation, field monitoring, and theoretical analysis to determine the reasonable width of the coal pillars in Lugou Coal Mine, and gave two principles for maintaining the stability of the gob-side entry with top coal; Guo *et al.* (2017) proposed bolt grouting and concrete wall synergistic control technology for coal pillar side. However, although many methods are adopted to study the stability of coal pillar, the coal pillar side still has large deformation due to the adjacent working face mining.

As for the coal side support, Zhao *et al.* (2020) proposed the composite support method of "shotcreting + grouting anchor bolt + anchor bolt + grouting anchor cable + anchor cable by the whole section layerdouble arch synergy reinforcement technology, effectively improving the surrounding rock stability of the roadway; combined with the effect of anchor cable coupling parameters on the ultimate bearing capacity of stone and concrete, Jing *et al.* (2018) proposed a joint reinforcement scheme of anchor cable reinforcement and grouting filling after wall; In order to control the large deformation of coal side in goaf, Zhang *et al.* (2020) proposed a grouting cable bolt support method which is better than end anchor support. Although there are many considerable achievements in the study of coal side support, the study on the reinforcement support of anchor deformed coal side is less, especially the lack of relevant theoretical basis.

During the working face mining, a large plastic zone is formed under the action of mining disturbance and support

*Corresponding author, Professor
E-mail: ang.li3399@gmail.com



ISSN: 2005-307X (Print), 2092-6219 (Online)

pressure of working face, many scholars researched the plastic fracture zone under support pressure. Yu *et al.* (2019) analyzed the stress-strain characteristics of the coal side by establishing the mechanical model of high support pressure, and put forward the theoretical calculation formula of the width of the coal side fracture zone; Chen *et al.* (2018) based on the equilibrium of the plastic zone, derived a new closed-form solution that considered properties of the coal and the support strength; Hou *et al.* (1989) gave the width of stress limit equilibrium zone of coal according to stress equilibrium theory of loose medium. Although the above literature considers the failure effect of support pressure on the coal side, there is little research on the theoretical analysis of the side anchorage body combined with side pressure.

This paper established the coal side anchorage support pressure distribution model, combined with the inelastic mechanics model, and proposed a theoretical analytical solution for anchor cable reinforcement on the coal pillar side. The anchor cable reinforcement of the 20 m section of coal pillars left in the 13512 working face of Wangcun coal mine in Chenghe mining area has achieved a positive effect, further verified the feasibility of the theory and provided a reference for the reinforcement anchoring of similar roadways.

## 2. Elastic-plastic ideal residual strain model of coal

From the literature, coal body destruction usually shows elastic-plastic flow deformation characteristics (Cai *et al.* 2018, Jiang *et al.* 2016, Park and Kim 2005, Grassl and Jirasek 2006). In order to avoid overcomplicating the model building, it is simplified to an elastic-plastic ideal residual strain model of coal, and the curve was divided into the elastic deformation area, the plastic softening area and the residual deformation area (Guo *et al.* 2018, Oliveira *et al.* 2020), as shown in Fig. 2.

### 2.1 Elastic deformation phase

At this phase, the coal body is deformed elastically by force and still satisfies the Mohr-Coulomb criterion, as


Fig. 1 The roof anchor cable embedded in the roadway top angle affected by coal pillar convergence deformation

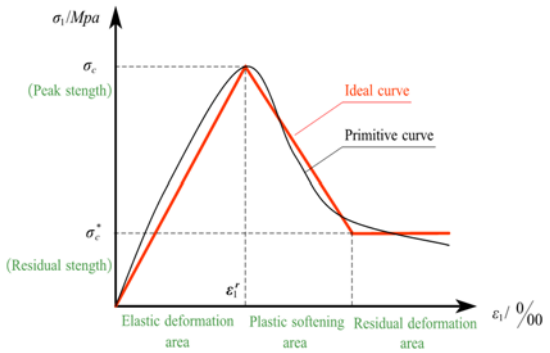


Fig. 2 Elastic-plastic ideal residual strain model of coal

$$\sigma_1 = k_p \sigma_3 + \sigma_c \tag{1}$$

Where $\sigma_c$ is the uniaxial compressive strength of coal, MPa, and $\sigma_c = \frac{2C\cos\varphi}{1-\sin\varphi}$; $\varphi$ is the internal friction angle of the coal seam, °; $C$ is the coal body cohesion, MPa.

### 2.2 Plastic softening phase

This phase of coal deformation conforms to the Mohr-Coulomb criterion, assuming a constant internal friction angle of coal, the strength of the coal reduces as the cohesion decreases, and its plastic softening condition is

$$\sigma_1 = k_p \sigma_3 + \sigma_c^p \tag{2}$$

$$\sigma_c^p = \sigma_c - M_0(\varepsilon_1 - \varepsilon_1^e) \tag{3}$$

Where $\sigma_c^p$ is plastic softening strength of coal, MPa; $\varepsilon_1^e$ is the maximum principal strain at yielding; $M_0$ is softening modulus, MPa, $M_0 = \tan\theta$.

### 2.3 Residual deformation phase

At this stage, the coal body deforms and disrupts, with a distinct decrease in strength, but the yield condition still satisfies the Mohr-Coulomb criterion, as

$$\sigma_1 = k_p^* \sigma_3 + \sigma_c^* \tag{4}$$

Where $k_p^* = \frac{1+\sin\varphi^*}{1-\sin\varphi^*}$, $\sigma_c^*$ is residual strength of the coal under uniaxial compression, MPa, $\sigma_c^* = \frac{2C^*\cos\varphi^*}{1-\sin\varphi^*}$; $C^*$ is residual cohesion of coal, MPa; $\varphi^*$ is residual friction angle, °.

## 3. Stress characteristics analysis of coal pillar anchorage section

After the coal seam is anchored, the coal mass and the anchor are tightly combined without relative sliding. Due to

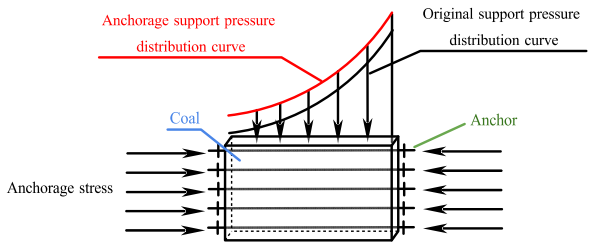


Fig. 3 Stress analysis diagram of the coal pillar anchorage section

the anchor effect, the strength of the anchorage body and especially the fractured coal in the surrounding rock is boosted. At this time, the yield criterion of the anchor at each phase still satisfies the Mohr-Coulomb criterion. With the increase of anchorage body strength, the vertical supporting stress of the coal seam is increased. The roof is no longer sinking due to the action of the coal anchor, and the surrounding rock becomes more stable, as shown in Fig. 3. The soft coal pillar is affected by the adjacent working face mining, which leads to severe deformation of the side and a large plastic failure range. Therefore, this paper assumed that the anchorage zone is a fracture zone.

The anchorage body yield condition is

$$\sigma_1 = k_{\mathrm{p}}^{\mathrm{g}}\sigma_3 + \sigma_{\mathrm{c}}^{\mathrm{g}} \tag{5}$$

Where $\sigma_{\mathrm{c}}^{\mathrm{g}}$ is the strength of the fractured coal body after anchoring, MPa, $\sigma_{\mathrm{c}}^{\mathrm{g}} = \frac{2C^{\mathrm{g}}\cos\varphi^{\mathrm{g}}}{1-\sin\varphi^{\mathrm{g}}}$; $C^{\mathrm{g}}$、$\varphi^{\mathrm{g}}$ are the residual cohesion and residual friction angle of coal, °.

Since the internal friction angle varies relatively little at each stage and has a weak effect on the strength of the coal body, it is assumed that the internal friction angle of coal is constant, as $\varphi^* = \varphi^{\mathrm{g}} = \varphi$, then $k_{\mathrm{p}}^* = k_{\mathrm{p}}^{\mathrm{g}} = k_{\mathrm{p}} = \frac{1+\sin\varphi}{1-\sin\varphi}$.

## 4. Mechanical model of support pressure distribution in coal pillar side

In the process of roadway excavation, the two sides of coal are damaged to varying degrees due to the influence of support pressure (Yang and Gou 2021, Du *et al.* 2020). The plastic failure zone of the section coal pillar is increased due to the superposition action of the advanced support pressure and the lateral support pressure near the mining face. This paper classifies the coal pillar side section into anchorage fracture zone, fracture zone, plastic zone, elastic zone and original rock stress zone according to the anchorage and non-anchorage zones of the anchor and the degree of coal fragmentation before and after the peak support pressure. In Fig. 4, The fracture zone, plastic zone and elastic zone of the anchorage support pressure distribution model correspond to the residual deformation phase, plastic softening phase, and elastic deformation phase of the elastic-plastic ideal residual strain model in Fig. 2, respectively. The yield criterion of the anchorage fracture zone also conforms to the Mohr-Coulomb criterion.

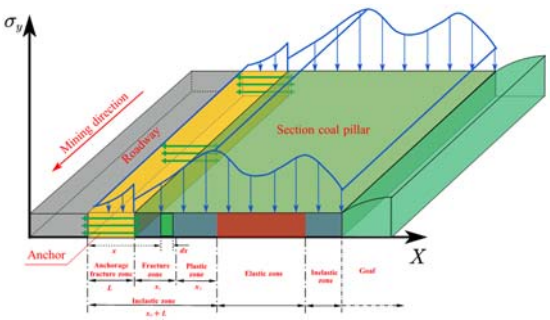


Fig. 4 section coal pillar anchorage support pressure distribution model

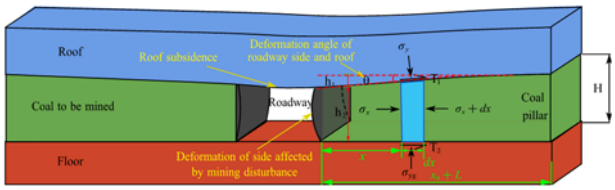


Fig. 5 Mechanical model of inelastic state

Therefore, the strain-softening characteristics of the coal body are used to study the distribution law of the anchorage support pressure and the reinforcement anchorage stress of the coal pillar.

## 5. Analysis of reinforcement anchorage stresses in the coal pillar side

### *5.1 Inelastic state mechanics model analysis*

According to the theory of mine pressure, the mechanical model of coal inelastic state is established by combining the stress condition in the inelastic area of the anchorage side. Then, the expression for the support pressure of the coal body in the inelastic area under the limit equilibrium state is obtained, and the expression for the anchorage stress of the surrounding rock is deduced.

Taking the unit with width *dx* for stress analysis, as shown in Fig. 5. In the case of ignoring gravity, the unit body meets the limit stress equilibrium condition under stress in each direction, and the following equilibrium equation can be listed

$$\Sigma F_{\mathrm{x}} = 0 \tag{6}$$

$$\Sigma F_{\mathrm{y}} = 0 \tag{7}$$

$$T_1 = C_1 + f_1\sigma_{\mathrm{y}} \tag{8}$$

$$T_2 = C_1 + f_1\sigma_{\mathrm{yg}} \tag{9}$$

From Eq. (6) the equilibrium equation for horizontal direction stress is established as follows

$$\sigma_{\mathrm{x}}(h_2 + x\tan\theta) - (\sigma_{\mathrm{x}} + d\sigma_{\mathrm{x}})[h_2 + (x+dx)\tan\theta] + T_1\cos\theta\frac{dx}{\cos\theta} + \sigma_{\mathrm{y}}\sin\theta\frac{dx}{\cos\theta} + T_2 dx = 0 \tag{10}$$

From Eq. (7) the equilibrium equation for vertical direction stress is established as follows

$$\sigma_{yg}dx + T_1 \sin\theta \frac{dx}{\cos\theta} - \sigma_y \cos\theta \frac{dx}{\cos\theta} = 0 \tag{11}$$

Where $\sigma_y$ is the normal stress of coal seam affected by the roof, MPa; $C_1$ is the cohesive force between coal seam and roof, MPa; $f_1$ is coal seam friction coefficient; $\theta$ is deformation angle of roadway side and roof, °; $H$ is the height of roadway, m, $H = h_1 + h_2$; $h_1$ is the deformation of coal side, m; $h_2$ is the height of coal after deformation, m; $\sigma_{yg}$ is the normal stress of coal seam affected by floor, MPa.

### 5.1.1 Anchorage fracture zone

From the previous analysis, it is known that the anchorage body yielding condition at this stage still satisfies the Mohr-Coulomb criterion. The compression of the coal side is smaller than the width of the plastic fracture zone, so the stress conditions of the micro-unit can be analyzed according to the inelastic state mechanical model. $\sigma_1$ and $\sigma_3$ in Eqs. (1), (2), (4), (5) can be substituted by $\sigma_{yg}$, $\sigma_x$ in micro-units. The critical condition of coal seam failure is

$$\sigma_{yg} = k_p^g \sigma_x + \sigma_c^g \tag{12}$$

After the coal seam is anchored, the anchor or anchor cable provides anchorage stress to the coal side. The boundary condition at this stage is

$$\sigma_x|_{x=0} = p \tag{13}$$

Rectifying Eqs. (8)-(12)

$$\sigma_y = \frac{k_p^g \sigma_x + \sigma_c^g + C_1 \tan\theta}{1 - f_1 \tan\theta} \tag{14}$$

$$\frac{d\sigma_x}{dx} + \frac{\sigma_x}{h_2 + x\tan\theta}\left[\tan\theta - k_p^g f_1 - \frac{k_p^g (f_1 + \tan\theta)}{1 - f_1\tan\theta}\right] - \frac{1}{h_2 + x\tan\theta}\left[2C_1 + f_1\sigma_c^g + \frac{(\sigma_c^g + C_1\tan\theta)(f_1 + \tan\theta)}{1 - f_1\tan\theta}\right] = 0 \tag{15}$$

To simplify the calculation, set

$$A = \left[\tan\theta - k_p^g f_1 - \frac{k_p^g (f_1 + \tan\theta)}{1 - f_1\tan\theta}\right]$$

$$B = \left[2C_1 + f_1\sigma_c^g + \frac{(\sigma_c^g + C_1\tan\theta)(f_1 + \tan\theta)}{1 - f_1\tan\theta}\right]$$

Then the Eq. (15) can be simplified as

$$\frac{d\sigma_x}{dx} + \frac{A}{h_2 + x\tan\theta}\sigma_x = \frac{B}{h_2 + x\tan\theta} \tag{16}$$

Taking the boundary condition Eq. (13) into Eq. (16) and solution gives

$$\sigma_x = \frac{B}{A} - \left(\frac{B}{A} - p\right)\left(\frac{h_2}{h_2 + x\tan\theta}\right)^{\frac{A}{\tan\theta}} \tag{17}$$

$$\sigma_y = \frac{Bk_p^g}{A} - \left(\frac{B}{A} - p\right)k_p^g\left(\frac{h_2}{h_2 + x\tan\theta}\right)^{\frac{A}{\tan\theta}} + \sigma_c^9 \tag{18}$$

$$\sigma_{yg} = \frac{BC}{A} - \left(\frac{B}{A} - p\right)C\left(\frac{h_2}{h_2 + x\tan\theta}\right)^{\frac{A}{\tan\theta}} + D \tag{19}$$

Where: $C = \dfrac{k_p^g}{1 - f_1\tan\theta}$, $D = \dfrac{\sigma_c^g + C_1\tan\theta}{1 - f_1\tan\theta}$

Since the deformation angle of the roadway roof and side is relatively small, therefore the Taylor expansion of $\theta$ in coefficients A, B, C, and D is carried out, taking the main valve and simplify it

$$A = [1 - k_p^g(1 + f_1^2)]\theta - 2k_p^g f_1$$

$$B = 2C_1 + 2f_1\sigma_c^g + \theta[C_1 f_1 + \sigma_c^g(1 + f_1^2)]$$

$$C = k_p^g(1 + f_1\theta)$$

$$D = \sigma_c^g + (C_1 + \sigma_c^g f_1)\theta$$

Substituting the above coefficients A, B, C, D into Eqs. (17)-(19), and the expressions of horizontal stress, vertical stress and supporting stress under the condition of coal anchorage are obtained by sorting out and taking the main value part as follows

$$\sigma_x = -\frac{C_1 + f_1\sigma_c^g}{k_p^g f_1} + \left[\frac{C_1 + f_1\sigma_c^g}{k_p^g f_1} + p\right]\left(1 + \frac{x\theta}{h_2}\right)^{\frac{2k_p^g f}{\theta}} \tag{20}$$

$$\sigma_y = \sigma_{yg} = \left[\frac{C_1 + f_1\sigma_c^g}{f_1} + pk_p^g\right]\left(1 + \frac{x\theta}{h_2}\right)^{\frac{2k_p^g f}{\theta}} - \frac{C_1}{f_1} \tag{21}$$

### 5.1.2 Fracture zone

Since the non-anchored fracture zone corresponds to the residual deformation phase of the elastic-plastic ideal residual strain model, $\sigma_1$ and $\sigma_3$ in Eqs. (1)、(2) and (4) can be substituted by $\sigma_{yg}$ and $\sigma_x$ in micro-units. The critical condition is

$$\sigma_{yg} = k_p^* \sigma_x + \sigma_c^* \tag{22}$$

According to the stress continuity condition of coal, the horizontal stress is equal at the anchorage zone $x = L$. The boundary condition is

$$\sigma_x|_{x=L} = -\frac{C_1 + f_1\sigma_c^g}{k_p^g f_1} + \left[\frac{C_1 + f_1\sigma_c^g}{k_p^g f_1} + p\right]\left(1 + \frac{L\theta}{h_2}\right)^{\frac{2k_p^g f_1}{\theta}} \tag{23}$$

Sorting Eqs. (10), (11) and (22), and substituting the boundary condition of the Eq. (23). The stress expressions under the fractured state of surrounding rock are obtained

$$\sigma_x = -\frac{C_1 + f_1\sigma_c^*}{k_p^* f_1} + \left\{\frac{\sigma_c^* - \sigma_c^g}{k_p^*} + \left[\frac{C_1 + f_1\sigma_c^g}{k_p^g f_1} + p\right]\left(1 + \frac{L\theta}{h_2}\right)^{\frac{2k_p^g f_1}{\theta}}\right\} \times \left[1 + \frac{(x - L)\theta}{h_2}\right]^{\frac{2k_p^* f_1}{\theta}} \tag{24}$$

$$\sigma_y = \sigma_{yg} = -\frac{C_1}{f_1} + \{\sigma_c^* - \sigma_c^g + \left[\frac{k_p^*[C_1 + f\sigma_c^g]}{k_p^g f_1} + pk_p^*\right]\left(1 + \frac{L\theta}{h_2}\right)^{\frac{2k_p^g f}{\theta}}\} \times \left[1 + \frac{(x - L)\theta}{h_2}\right]^{\frac{2k_p^* f_1}{\theta}} \tag{25}$$

### 5.1.3 Plastic zone

Due to the small plastic zone and the little roof

subsidence in the elastic-plastic ideal residual strain model of the coal body, and its stress state is consistent with the inelastic state mechanical model. The plastic zone strain $\varepsilon_1$ has the following relationship equation

$$\varepsilon_1 = \varepsilon_1^{\mathrm{p}} + \varepsilon_1^{\mathrm{e}} = \frac{[(x_0+L)-(x+L)]}{H}\tan\theta + \varepsilon_1^{\mathrm{e}} \tag{26}$$

Where $\varepsilon_1^{\mathrm{e}}$ is plastic deformation.

$\sigma_1$ and $\sigma_3$ in Eqs. (1) and (2) can be substituted by $\sigma_{yg}$, $\sigma_x$ in micro-units. The critical condition is

$$\sigma_{\mathrm{yg}} = k_{\mathrm{p}}\sigma_{\mathrm{x}} + \sigma_{\mathrm{c}}^{\mathrm{p}} \tag{27}$$

Substituting Eqs. (3) and (26) into (27) gives

$$\sigma_{\mathrm{yg}} = \sigma_{\mathrm{x}}k_{\mathrm{p}} + \sigma_{\mathrm{c}} - M_0\frac{x_0+L-x}{H}\tan\theta \tag{28}$$

According to the stress continuity condition for the plastic and fracture zones, when $x=x_1+L$, the width of the plastic zone is

$$x_2 = \frac{\sigma_{\mathrm{c}}-\sigma_{\mathrm{c}}^*}{M_0 tan\theta}H \approx \frac{\sigma_{\mathrm{c}}-\sigma_{\mathrm{c}}^*}{M_0\theta}H \tag{29}$$

The boundary condition is

$$\sigma_{\mathrm{x}}\big|_{x=x_1+L} = -\frac{C_1+f_1\sigma_{\mathrm{c}}^*}{k_{\mathrm{p}}^* f_1} + \left\{\frac{\sigma_{\mathrm{c}}^*-\sigma_{\mathrm{c}}^{\mathrm{g}}}{k_{\mathrm{p}}^*} + \left[\frac{C_1+f_1\sigma_{\mathrm{c}}^{\mathrm{g}}}{k_{\mathrm{p}}^* f_1}+p\right]\left(1+\frac{L\theta}{h_2}\right)^{\frac{2k_{\mathrm{p}}^* f_1}{\theta}}\right\}\times \left[1+\frac{x_1\theta}{h_2}\right]^{\frac{2k_{\mathrm{p}}^* f_1}{\theta}} \tag{30}$$

Organize Eqs. (10), (11) and (28), solve the differential equations and substitute Eq. (30) for boundary conditions. Among them, $k_{\mathrm{p}}^* = k_{\mathrm{p}}^{\mathrm{g}} = k_{\mathrm{p}}$, and due to $\theta$ is two orders of magnitude smaller than $h_1$, so set $\frac{h_2+(x-L)\theta}{h_2+x_1\theta} \approx 1$. Therefore, the expressions of horizontal stress $x$, vertical stress $y$ and support pressure $z$ under plastic state are

$$\sigma_{\mathrm{x}} = -\frac{C_1+f_1\sigma_{\mathrm{c}}^*}{k_{\mathrm{p}}f_1} + \left\{\frac{\sigma_{\mathrm{c}}^*-\sigma_{\mathrm{c}}^{\mathrm{g}}}{k_{\mathrm{p}}} + \left[\frac{C_1+f_1\sigma_{\mathrm{c}}^{\mathrm{g}}}{k_{\mathrm{p}}f_1}+p\right]\left(1+\frac{L\theta}{h_2}\right)^{\frac{2k_{\mathrm{p}}f_1}{\theta}}\right\}\times \left[1+\frac{(x-L)\theta}{h_2}\right]^{\frac{2k_{\mathrm{p}}f_1}{\theta}} \tag{31}$$

$$\sigma_{\mathrm{y}} = \sigma_{\mathrm{yg}} = -\frac{C_2}{f_1} + \sigma_{\mathrm{c}} - \sigma_{\mathrm{c}}^* + \left\{\sigma_{\mathrm{c}}^*-\sigma_{\mathrm{c}}^{\mathrm{g}} + \left[\frac{[C_1+f_1\sigma_{\mathrm{c}}^{\mathrm{g}}]}{f_1} + pk_{\mathrm{p}}\right]\left(1+\frac{L\theta}{h_2}\right)^{\frac{2k_{\mathrm{p}}f}{\theta}}\right\}\left[1+\frac{(x-L)\theta}{h_2}\right]^{\frac{2k_{\mathrm{p}}f_1}{\theta}} - M_0\frac{x_0+L-x}{H}\tan\theta \tag{32}$$

### *5.2 Calculation of reinforcement anchorage stress for coal pillar side anchor cables*

The anchorage stress $p$ is the anchorage force provided by the anchor or anchor cable of the unit area required under stable coal conditions. According to the comparative analysis of the actual anchorage stress of the section coal pillar, the design specification of coal pillar reinforcement support can be determined. To calculate the anchorage stress $p$, it is assumed that the peak support pressure $P_1$ of coal at the junction of the elastic region and plastic region is

$$P_1 = K\gamma H_1 \tag{33}$$

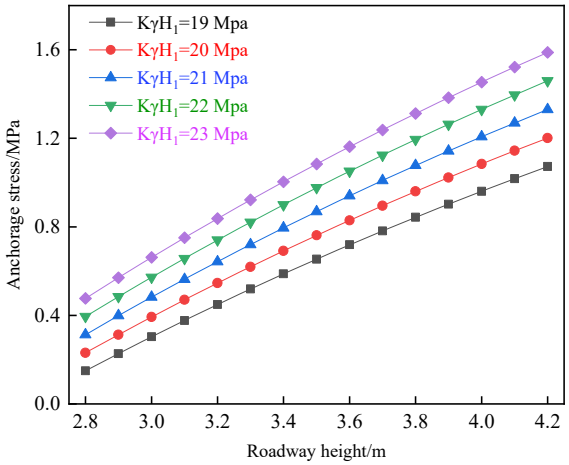


Fig. 7 Relationship between roadway height and anchorage stress under different peak support pressure

Where $K$ is support pressure peak coefficient; $\gamma$ is average volume weight of overlying strata, N/m$^3$; $H_1$ is buried depth of working face, m.

Substituting Eq. (33) into Eq. (32), the actual coal seam deformation angle $\theta$ is small, resulting in $h_1$ is smaller relative to $H$, so set $\mathrm{h_1} \approx \mathrm{H}$ $h_1 \approx H$ Then the reinforcing anchorage stress $p$ is

$$p = \frac{\xi\left(K\gamma H_1 + \frac{C_1}{f_1} + \sigma_{\mathrm{c}}^* - \sigma_{\mathrm{c}}\right) - \sigma_{\mathrm{c}}^* + \sigma_{\mathrm{c}}^{\mathrm{g}} - \left(\frac{C_1}{f_1} + \sigma_{\mathrm{c}}^{\mathrm{g}}\right)\psi}{k_{\mathrm{p}}\psi}$$
$$\psi = \left(1+\frac{L\theta}{h_2}\right)^{\frac{2k_{\mathrm{p}}f_1}{\theta}} \tag{34}$$
$$\xi = \left(1+\frac{x_0\theta}{h_2}\right)^{-\frac{2k_{\mathrm{p}}f_1}{\theta}}$$

Where $x_0$ is width of plastic fracture zone, m.

## 6. Analysis of parameter influencing factors

### *6.1 Relationship between the deformation angle of roadway side and roof and the width of the plastic fracture zone at different anchorage stress*

Set the relevant parameters: peak support pressure $K\gamma H_1$ is 17 MPa, coal strength $\sigma_c$ is 4.25 MPa, residual strength $\sigma_{\mathrm{c}}^*$ is 0.15 MPa, $k_p$ is 3.1, coal seam and roof friction coefficient is 0.25, coal seam and roof and floor contact cohesion $C_1$ is 0.4 MPa, roadway height $H$ is 3.1 m, anchor length $L$ is 1.8 m, and anchorage body strength in the fracture zone $\sigma_{\mathrm{c}}^{\mathrm{g}}$ is 3.3 MPa. The following influence parameter curves can be obtained by substituting the above parameters into Eq. (34).

As shown in Fig. 6, the deformation angle of the roadway roof and side is the angle formed by roof subsidence and plastic zone width of the coal pillar. Due to the influence of working face mining, the coal side of the mining roadway is compressed downward by the disturbance, and the deformation angle increases. The

roadway surrounding rock rupture degree also intensifies, and in severe can lead to anchor fracture and extensive failure of the support. It can also be seen from the curves of different anchorage stress in the figure that increasing the anchor strength is important to reduce the sinking of the roadway roof, reducing the convergence of the side, inhibiting the deterioration of the plastic zone of the surrounding rock and controlling the stability of the surrounding rock.

### *6.2 Relationship between roadway height and anchorage stress under different peak support pressure*

Set the relevant parameters: deformation angle $\theta$ is 2°, dudcoal strength $\sigma_c$ is 4.25 MPa, residual strength $\sigma_c^*$ is 0.15 MPa, $k_p$ is 3.1, coal seam and roof friction coefficient is 0.25, coal seam and roof and floor contact cohesion $C_1$ is 0.4 MPa, the anchor length is 1.8 m, anchorage body strength in the fracture zone $\sigma_c^g$ is 3.3 MPa, and the width of the plastic fracture zone is 0.7 m. By substituting the above parameters into Eq. (34), the following influence parameter curves can be obtained.

As shown in Fig. 7, the anchorage stress required for the coal side increases with the height of the roadway. For roadways with higher heights, the coal side is more susceptible to flaking and the required anchorage stress consequently increases. The peak support pressure is also positively correlated with anchorage stress. As the depth of the coal seam increases, the surrounding rock of the roadway is in a high-stress state, and the coal wall bulging increases. Therefore, for coal seam mining with higher burial depth and higher roadway height, the anchorage strength of the coal pillar side should be increased in time to prevent the plastic zone of the coal side from extending further to the depth. The adjustment of the anchorage strength required by roadway surrounding rock can also be made by changing the support pressure coefficient $k$ under the condition that the burial depth of the roadway and the overburden weight remain unchanged. Moreover, using narrow coal pillar or non-coal pillar mining to avoid the peak bearing pressure area can effectively reduce the support pressure coefficient $k$, thus reducing the cost of rock support and maintenance. However, for mines affected by high confined water and serious water accumulation in goaf, it is more appropriate to leave wider coal pillars to eliminate the effects of water disaster during working face mining, as the 13512 workings in Wangcun coal mine. So increasing the anchorage strength is an important factor in protecting the stability of the roadway.

### *6.3 Relationship between cohesion and anchorage stress between coal seam and roof and floor under different length of anchor*

Set the relevant parameters: deformation angle $\theta$ is 2°, peak support pressure $K\gamma H_1$ is 20 MPa, coal strength $\sigma_c$ is 4.25 MPa, residual strength $\sigma_c^*$ is 0.15 MPa, $k_p$ is 3.3, coal seam and roof friction coefficient is 0.1, roadway height $H$ is 3.1 m, anchorage body strength in the fracture zone $\sigma_c^g$ is 3.3 MPa, and the width of the plastic fracture zone is 0.7 m. The following influence parameter curves can be obtained by substituting the above parameters into Eq. (34).

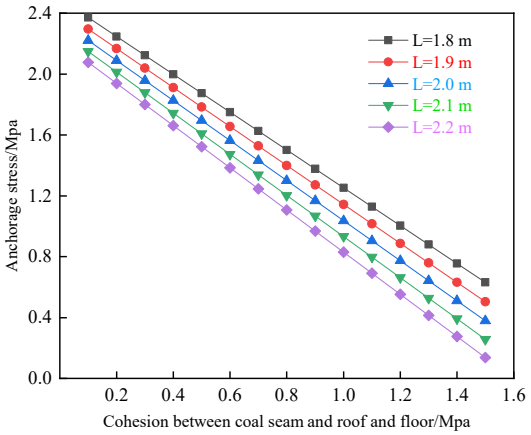


Fig. 8 Relationship between cohesion and anchorage stress between coal seam and roof and floor under different length of anchor

As shown in Fig. 8, the required anchorage stress of the coal side decreases as the cohesion between the coal seam and the roof and floor increases. As the cohesion increases, the coal pillar side becomes more stable and the required coal side anchorage stress decreases. In addition, the graph also shows that the anchor length is inversely proportional to the anchorage stress required for the coal pillar side. That is, the anchor length also has an essential effect on increasing the strength of the anchorage body. Therefore, the coal cohesion should be improved when anchoring the coal side, and the length of anchor or anchor cables should be selected to be approximately or more than the width of the inelastic zone to enhance the stability of the surrounding rock. The cohesion strengthening methods of coal seam and roof and floor include encryption anchor, reinforcement anchor cable and slurry reinforcement, but the cost of slurry reinforcement is substantially higher and the slurry is more susceptible to leak. From the perspective of roadway maintenance time and comprehensive cost, the choice of anchor cable reinforcement is more effective than encryption anchor rods alone.

## 7. Engineering application

### *7.1 Engineering background*

The 13512 working face of No. 5 coal seam in Wangcun coal mine of Chenghe mining area has formed goaf, and the width of section coal pillar is set to 20 m. The coal seam is buried at 300 m, with an average thickness of 4 m. The coal is soft and loose. The roadway is the rectangular layout, with a width × height of 4.8 m × 3.1 m. The side uses Φ18 × 1800 mm left-hand threaded steel resin anchors, five on each side with an inter-row distance of 700 mm × 800 mm and an anchorage force of not less than 60 kN. The original design of roadway support is shown in Fig. 9.

Table 1 Uniaxial compressive strength critical load test value

| Measuring station | Drilling depth/m | Critical load $\sigma_p$/MPa | Uniaxial compressive strength $\sigma_i$/MPa | |
|---|---|---|---|---|
| | | | calculated value | mean value |
| First measuring station | 0.6 | 2.108 | 3.427 | 3.3 |
| | 1.2 | 1.932 | 3.285 | |
| | 1.8 | 1.676 | 3.079 | |
| Second measuring station | 0.6 | 2.238 | 3.532 | |
| | 1.2 | 1.784 | 3.166 | |
| | 1.8 | 1.956 | 3.304 | |
| Third measuring station | 0.6 | 1.860 | 3.227 | |
| | 1.2 | 1.848 | 3.217 | |
| | 1.8 | 2.153 | 3.463 | |

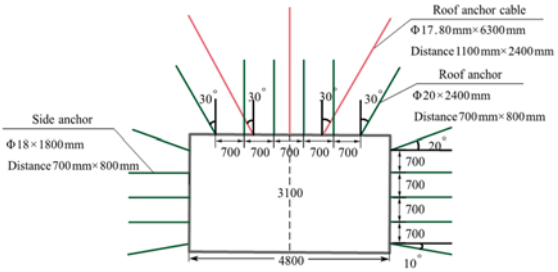


Fig. 9 Original support design diagram of mining roadway

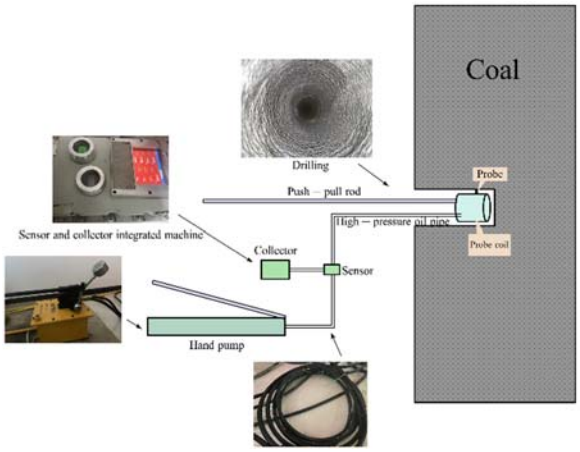


Fig. 10 Principle diagram of coal rock mass strength test

The preliminary investigation found that the original support anchor in the coal pillar side of the transportation roadway has serious roof subsidence and convergence deformation of the two sides, the most serious part of the side was squeezed inwards by 0.4 m. The roof anchor cable is squeezed into the roof angle of the roadway by the convergence deformation of the side as shown in Fig. 1. The coal body in the sidewall is squeezed into the roadway, which seriously affects the regular use of the roadway. By monitoring the borehole peep and deformation of the surrounding rock, the existing anchor support system is insufficient to control the convergence deformation of the surrounding rock. The proposed anchor cable reinforcement technology is used to manage the roadway side and stabilize the roof, but there is a lack of theoretical basis for the corresponding side reinforcement support parameters. Therefore, the theoretical research of this paper is used to guide the field engineering practice and solve the technical parameters such as the length, diameter and inter-row distance of the side anchor reinforcement.

### *7.2 Uniaxial compressive strength test of anchorage body of section coal pillar*

As the uniaxial compressive strength of the anchored fracture zone needed to be measured, a borehole rock strength in-situ tester was selected (Zhang 2020), which consisted of a probe coil, hand pump, high-pressure oil pipe, push-pull rod, sensor, and collector, as shown in Fig. 10. The measurement is carried out by drilling a hole in the coal side and pressurizing the probe placed in the hole, at which point the probe applies pressure to the coal seam until the coal body ruptures and the ultimate pressure value is recorded. After conversion with the uniaxial compressive strength of the rock sample in the laboratory, the uniaxial compressive strength of the coal body can be obtained.

Three groups of stations were arranged in the section coal pillar of 13512 working face, with a distance of 50 m. A horizontal borehole was arranged in each station with a depth of 2 m and a diameter of 56 mm. Each station was equipped with one horizontal borehole with a depth of 2 m and a diameter of 56 mm, and each borehole set three measurement points with a spacing of 0.6 m. When the critical load value of the instrument test coal sample is 1.5 – 3.5 MPa, the uniaxial compressive strength of coal could be obtained by the following equation (Lei *et al.* 2019)

$$\sigma_i = 0.807\sigma_p + 1.726 \tag{35}$$

Where $\sigma_i$ is the uniaxial compressive strength of coal, MPa, applicable range 1.5 ~ 3.5 MPa; $\sigma_p$ is measuring critical loads for instruments, MPa.

The test results and uniaxial compressive strength are shown in Table 1, so the average uniaxial compressive strength of coal in the anchorage fracture area is 3.3 MPa.

### *7.3 Anchorage stress analysis of coal pillar in 13512 working face*

Substituting the parameters in Table 2 into Eq. (34) gives a theoretical unit anchorage stress required for the coal side is p=0.174 MPa, which is greater than the actual unit anchorage stress of 0.121 MPa in the field anchor

Table 2 The value of each parameter

| Raw date | | | | | | | Measured data | | | | Calculated value |
|---|---|---|---|---|---|---|---|---|---|---|---|
| Parameter | $\theta$ | $K\gamma H_1$ | $L$ | $H$ | $f_1$ | $C_1$ | $\sigma_c$ | $\sigma_c^g$ | $\sigma_c^*$ | $x_0$ | $k_p$ |
| | /° | /MPa | /m | /m | | /MPa | /MPa | /MPa | /MPa | /m | |
| Value | 2 | 17.3 | 1.8 | 3.1 | 0.33 | 0.5 | 4.25 | 3.3 | 0.15 | 0.71 | 3.39 |


Fig. 11 Effect diagram of anchor cable reinforcement in the section coal pillar side

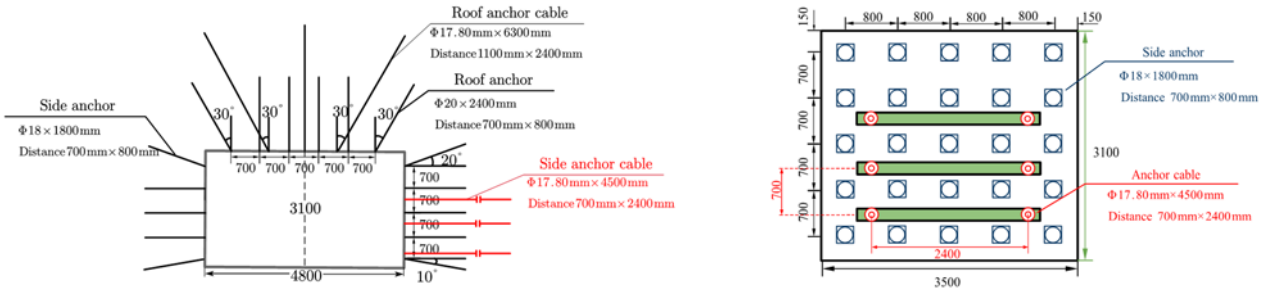


(a) Front view of side anchor cable reinforcement design

(b) Lateral view of side anchor cable reinforcement design

Fig. 12 Diagram of anchor cable reinforcement of mining roadway

specifications. From the previous theoretical analysis, it can be seen that the length of the anchor or anchor cable should exceed 2.5 m of the width of the inelastic zone when reinforcing and anchoring the coal side. Considering the previous increase in anchor reinforcement often failed to achieve the desired effect and the free end of the anchor was unable to anchor the inelastic zone of the coal side fully, anchor cables were selected to reinforce the coal side in the mining roadway. According to Eqs. (36) and (37), three anchor ropes are required to reinforce the coal side within an area of 7.44 m$^2$. The anchor cables are 4.5 m in length, designed with Φ17.8 mm×4500 mm left-handed strand, with an anchorage force of not less than 150 kN and an inter-row spacing of 700 mm×2400 mm, connected by steel beams in the middle. The anchorages are placed at 2.1 m, 1.4 m and 0.7 m from the roadway floor, as shown in Figs. 11, 12(a) and 12(b). The existing anchorage stress in the roadway side is 0.181 MPa after the anchor cable is added, which is slightly higher than the theoretical anchorage value of 0.174 MPa.

$$P - \frac{F_c N_c}{S} \leqslant \frac{F_k N_k}{S} \tag{36}$$

$$L = L_1 + c + L_2 \tag{37}$$

Where $P$ is the unit anchorage stress, MPa; $F_c$ is the anchorage force provided by the anchor, kN; $N_c$ is the anchor quantity in the intercepted area; $S$ is the intercepted area of the coal side, m$^2$; $F_k$ is the anchorage force provided by the anchor cable, kN; $N_k$ is the anchor cable quantity in the intercepted area; $L$ is the anchor cable length, m; $L_1$ is the exposed length of the anchor cable, generally selected as 0.35 m; $c$ is the length of the external anchorage section of the anchor cable, namely 2.51 m of the length of the inelastic zone; $L_2$ is the length of the inner anchorage section, selected as 1.64 m.

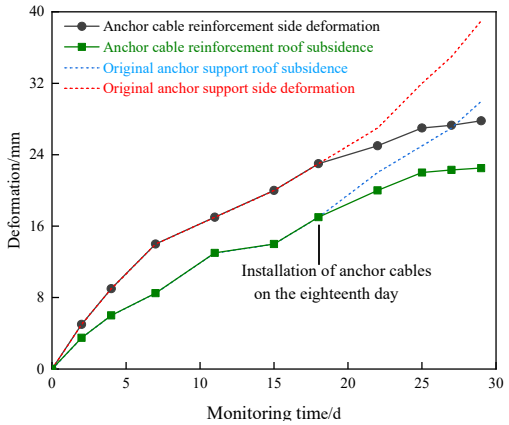


Fig. 13 Roadway deformation monitoring

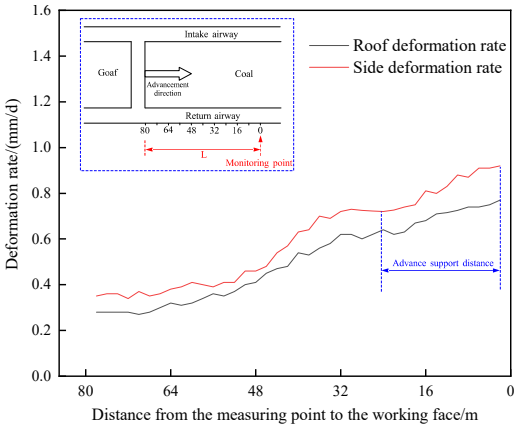


Fig. 14 Monitoring of side deformation rates after anchor cable reinforcement

### *7.4 Analysis of the roadway support effect*

As shown in Fig. 13, the dashed line is the predicted original roof and side deformation and the solid line is the roof and side deformation of the roadway after anchor cable anchoring. When the 18 the day of roadway measurement found that the width of the coal inelastic zone generally reached 2.5 m, and the deformation of the roadway side was always increasing. After adding anchor cables to the coal pillar side for reinforcement, the roof subsidence trend and the roadway convergence deformation decreased significantly, and the growth of the plastic fracture zone of coal gradually stabilized. The displacement rate of roadway roof and side after anchor cable anchorage is monitored as shown in Fig. 14. Displacement monitoring points were arranged at 80 m from the working face. As the working face advanced, the deformation rate of the side and the roof is increasing, but the growth trend is consistently slow. Until the working face advanced to the monitoring point, the displacement rate of the roof and the side is only 0.77 mm/d and 0.92 mm/d, which is far from reaching the failure support range of the anchor cable. The deformation of the roadway side and the roof is within the controllable range. So the support method further verifies the feasibility of the theory, effectively controlling the deformation of the roadway surrounding rock and ensuring the smooth mining of the working face.

## 8. Conclusions

This paper, based on the coal elastic-plastic strain-softening model, establishes the anchorage body support pressure distribution model. The distribution law of support pressure of anchor coal side is studied by using the strain-softening characteristics of coal body. Combined with the inelastic mechanical model, derives the coal side anchor cable reinforcement anchorage stress analytical solution, and obtains the following conclusions:

- The deformation angle of the roadway side and roof is generally affected by mining disturbance, resulting in enlarged width of the plastic zone. The roadway height and the coal seam depth increase, causing the coal pillar side to deflect easily, enhancing the anchorage strength can effectively control the roadway surrounding rock convergence deformation.
- For the secondary reinforcement of the section coal pillar, it should be supplemented by a high pre-stressed anchor cable which can pass through the plastic zone of the side or by strengthening the anchor length and cohesion, to control the plastic failure depth of the side and provide a better reinforcement effect.
- Under the condition of constant roadway depth and overburdened bulk density, the support pressure coefficient can be effectively reduced by using narrow coal pillar or non-coal pillar mining to avoid the peak area of support pressure to reduce the cost of support pressure surrounding rock support.
- Based on the theoretical, the anchor cable reinforcement support design is carried out for coal pillars affected by mining disturbance in Wangcun coal mine section pillar side in Chenghe mining area. The displacement monitoring of the roadway floor and the coal pillar side was carried out on-site, which achieved great results and effectively controlled the deformation of the roadway surrounding rock, further verifying the reasonableness of the formula.

## Acknowledgements

The authors are grateful for financial assistance provided by the National Natural Science Foundation of China (Nos. 41402265 and 51874229) and the Natural Science Foundation of Shaanxi Province (2020JZ-52).

## References

Cai, W., Dou, L.M., Ju, Y., Cao, W.Z., Yuan, S.S. and Si, G.Y. (2018), "A plastic strain-based damage model for heterogeneous coal using cohesion and dilation angle", *Int. J. Rock Mech. Min. Sci.*, **110**, 151-160. https://doi.org/10.1016/j.ijrmms.2018.08.001.

Chen, D.G., Gao, Z.N., Zhao, G.M., Li, S.S. and Zhao, C.X. (2020), "Stability analysis of surrounding rock under anchorage mechanics effect", *J China Coal Soc.*, **45**(3), 1009-1019. https://doi.org/10.13225/j. cnki. jccs. SJ19. 1819.

Chen, S.J., Qu, X., Yin, D.W., Liu, X.Q. and Ma, H.F. and Wang, H.Y. (2018), "Investigation lateral deformation and failure characteristics of strip coal pillar in deep mining", *Geomech. Eng.*, **14**(5), 421-428.

https://doi.org/10.12989/gae.2018.14.5.421.
Cheng, L. and Zhang, Y.D. (2018), "A new closed-form solution of the side abutment pressure distribution of roadway", *Adv Civ Eng.*, 2018, 1-10. https://doi.org/10.1155/2018/1409493.
Du, B.J., Liu, C.Y., Yang, J.X. and Wu, F.F. (2020), "Abutment pressure distribution pattern and size optimization of coal pillar under repeated mining: a case study", *Arab. J. Geosci.*, **13**(23), 1261. https://doi.org/10.1007/s12517-020-06281-y.
Gao, W. (2018), "Influence of interaction between coal and rock on the stability of strip coal pillar", *Geomech. Eng.*, **16**(2), 151-157. https://doi.org/10.12989/gae.2018.16.2.151.
Grassl, P. and Jirasek, M. (2006), "Damage-plastic model for concrete failure", *Int. J. Solids Struct*., **48**(22-23), 7166-7196. https://doi.org/10.1016/j.ijsolstr.2006.06.032.
Guo, W.Y., Tan, Y.L., Yu, F.H., Zhao, T.B., Hu, S.C., Huang, D.M. and Qin, Z. (2018), "Mechanical behavior of rock-coal-rock specimens with different coal thicknesses", *Geomech. Eng*., **15**(4), 1017-1027. https://doi.org/10.12989/gae.2018.15.4.1017.
Guo, J.G., Wang, W.G., Yue, S.S., He, F.L., Gao, M.M. and Xie, S.G. (2017), "Surrounding rock control mechanism and its application of gob-side driving entry in extra thick coal seam", *J China Coal Soc.*, **42**(4), 825-832. https://doi.org/10.13225/j.cnki.jccs.2016.1571.
Hou, C.J. and Ma, N.J. (1989), "Stress in in-seam roadway sides and limit equilibrium zone", *J China Coal Soc.*, **4**, 21-29. https://doi.org/10.13225/j.cnki.jccs.1989.04.003.
Jiang, L., Sainoki, A., Mitri, H.S., Ma, N.J., Liu, H.T. and Hao, Z. (2016), "Influence of fracture-induced weakening on coal mine gateroad stability", *Int. J. Rock Mech. Min. Sci*., **88**, 307-317. https://doi.org/10.1016/j.ijrmms.2016.04.017.
Jing, S.G., Su, Z.L. and Wang, X.K. (2018), "Research and application on the coupling mechanism of cable and masonry for chamber with large-section", *J. Min. Safety Eng.*, **35**(6), 1158-1163. https://doi.org/10.13545/j.cnki.jmse.2018.06.010.
Lei, S., Kang, H.P., Gao, F.Q. and Si, L.P. (2019), "Study and application of a method for rapid-determination of uniaxial compressive strength of weak coal in Xinyuan coal mine", *J. China Coal Soc.*, **44**(11), 3412-3422. https://doi.org/10. 13225 /j. cnki. jccs. 2018. 1622.
Li, A., Ma, Q., Lian, Y., Lian, Y.Q., Ma, L., Mu, Q. and Chen, J.B. (2020a), "Numerical simulation and experimental study on floor failure mechanism of typical working face in thick coal seam in Chenghe mining area of Weibei, China", *Environ. Earth. Sci.*, **79**(5), 118. https://doi.org/10.1007/s12665-020-8839-2.
Li, A., Ma, Q., Ma, L., Kang, L., Mu, Q. and Chen, J.B. (2020b), "Coal mine abutment pressure distribution based on a strain-softening model", *Front. Phys.*, **8**, 263. https://doi.org/10.3389/fphy.2020.00263.
Ma, Z.Q., Chen, C., Liang, X.C., Chen, A.M. and Song, W.X. (2020), "Field and numerical investigation on the stability of coal pillars of gob-side entry driving with top coal", *Arab. J. Geosci.*, **13**(22), 1193. https://doi.org/10.1007/s12517-020-06234-5.
Oliceira, D.B., Penna, S.S. and Pitangueira, R.L.S. (2020), "Elastoplastic constitutive modeling for concrete: a theoretical and computational approach", *Geomech. Eng*., **13**(1), 171-182.
https://doi.org/10.1590/S1983-41952020000100012.
Park, H. and Kim, J.Y. (2005), "Plasticity model using multiple failure criteria for concrete in compression", *Int. J. Solids Struct.*, **42**(8), 2303-2322. https://doi.org/10.1016/j.ijsolstr.2004.09.029.
Wattimena, R.K., Kramadibrata, S., Sidi, I.D. and Azizi, M.A. (2013), "Developing coal pillar stability chart using logistic regression", *Int. J. Rock Mech. Min. Sci*., **58**, 55-60. https://doi.org/10.1016/j.ijrmms.2012.09.004.
Wei, P., Liang, Y., Zhao, S., Peng, H.J., Li, X.L. and Meng, R. (2018), "Characterization of pores and fractures in soft coal from the No. 5 soft coalbed in the Chenghe mining area", *Processes*, **7**(1), 13. https://doi.org/10.3390/pr7010013.
Yang K, Gou PF. (2021), "Research on reasonable width of coal pillars in high strength mining roadway in Wantugou Mine", *Geotech. Geol. Eng.*, **39**(3), 2065-2073. https://doi.org/10.1007/s10706-020-01607-9.
Yu, Y.X., Ke, D., Wang, J.B., Wang, B.Y. and Chen, B.P. (2019), "A discussion on determination method of the limit equilibriumzone width based on the deformation analysis of coal wall", *J China Coal Soc.*, **44**(11), 3340-3348. https://doi.org/10. 13225/j.cnki.jccs.2018.1600.
Zhang F. (2020), "Strength test and supporting parameters design of roadway surrounding rock in coal mine", *China Energy Environ Prot.*, **42**(10), 192-195. https://doi.org/10.19389/j.cnki.1003 -0506. 2020. 10. 040.
Zhao, C.X., Li, Y.M., Liu, G. and Meng, X.R. (2020), "Mechanism analysis and control technology of surrounding rock failure in deep soft rock roadway", *Eng Fail Anal.*, **115**, 104611. https://doi.org/10.1016/j.engfailanal. 2020.104611.
Zhang, Z.Y., Guan, W.M. and Chen, H. (2020), "Numerical study on the effectiveness of the grouting cable bolt in deep retained goaf side gateroad", *Geotech. Geol. Eng.*, **38**(5), 4529-4543. https://doi.org/10.1007/ s10706-020-01307-4.

*CC*